FOS Instrument Science Report CAL/FOS 146

The FOS Dark Count-rate: Cycles 1 to 4

Jeffrey J.E. Hayes and Don J. Lindler
December 19, 1996

ABSTRACT

This document gives an analysis of all FOS dark observations taken on-orbit from Cycle 1 through Cycle 4. We find that overall, the FOS/RED dark count-rate is 0.0109 $\pm$ ***0.0022*** cts s^{-1} diode^{-1}***, while for the FOS/BLUE, the count-rate is 0.0064*** $\pm$ ***0.00083*** cts s^{-1} diode^{-1}***. We confirm the finding of Rosenblatt*** *et al.* ***(1992) of the correlation between dark count-rate and geo-magnetic latitude, but see no evidence for any correlation between geo-magnetic longitude, solar position angle, or solar cycle. STScI is in the process of making a dark count-rate model suitable for both the GHRS and the FOS, which will be used in the pipeline.***

1 Introduction

The Faint Object Spectrograph (FOS) has two Digicons detectors with independent optical paths. The Digicons operate by accelerating photoelectrons emitted by a transmissive photocathode onto a linear array of 512 diodes. The individual diodes are 0.″31 wide by 1.″29 high perpendicular to the dispersion (Post-COSTAR). These detectors are subject to 2 types of backgrounds: 1) a so-called “dark current”; and 2) a particle induced background. The “dark current” is thermionic in nature and was measured in ground-based thermal vacuum tests to be 0.0003 cts s^{-1} diode^{-1} (Beaver and Lyons 1992; CAL/FOS-076). This was below the instrument specification at the time of launch. The second background source mentioned is that of the particle induced background, which will be the focus of the present paper.

2 Dark Count-rate

The dark count-rate, caused by high energy particles, can be broken into two distinct classes. One may have Čerenkov radiation, as particles hit the photocathode, or one may have the particles themselves striking one of the detectors. In either case, one will have extra photoelectrons in a given science observation that will enhance the noise content of the detected signal. As the dark count-rate is caused by charged high energy particles, it would appear reasonable to expect a geomagnetic positional dependence on the number of spurious counts detected. Indeed, Rosenblatt *et al.* (1992; CAL/FOS-071) found that there was a very marked difference in the particle-induced count-rate inside the South Atlantic Anomaly (SAA), than outside of it. The difference amounts to roughly 2 orders of magnitude. It is (partly) for this reason that *no* FOS observations are carried out in the SAA.

This dark count-rate background is the limiting factor in allowing faint objects to be studied. A V $\sim$ 19 star of T_e= 10000 K will have approximately the same count-rate as the dark count-rate for the FOS/RD detector + G270H grating, so obviously faint objects will be most significantly affected.

3 The Data

For the purposes of this report, we have pulled all 1491 dark datasets taken with the FOS from Cycles 1 through 4. All these datasets have REJLIM=0, the default value for the High Voltage, and were taken in IMAGE mode. Typically each dataset consists of 15 groups. In Table 1, we list the programmes from which the datasets were taken and the number of datasets per detector.

The datasets as pulled from the Archive were converted to GEIS format and occupy roughly 520MB.

4 Data Analysis

All of the datasets were analysed using the IRAF/STSDAS package. The dark count-rates were calculated using the STSDAS task "`parthity`", which used the C1H datasets. The task determines the average count rate per diode, using all the frames in the dataset. Points determined to be particle hits are not used in the average. Noisy diodes are identified as those having a dark count-rate greater than a given threshold: on the advice of D. Lindler, we used 4σ above the average for all diodes. Indeed, during our initial analysis for these data, we noted a "quantization" in the calculated dark count-rates. It was subsequently discovered that "`parthity`" must be used with caution, as setting the particle hit threshold too low will underestimate the dark count-rate and produce an artificial quantum effect in the data.

Table 1: FOS Dark datasets by cycle and detector.

Proposal ID	Detector	No. Datasets	Cycle
1316	FOS/RED	592	1
1316	FOS/BLUE	497	1
1533	FOS/RED	32	1
1533	FOS/BLUE	32	1
2748	FOS/RED	62	2
2748	FOS/BLUE	94	2
4698	FOS/RED	35	3
4698	FOS/BLUE	19	3
4773	FOS/RED	2	SMOV
5532	FOS/RED	67	4
5532	FOS/BLUE	69	4

For this reason, on the advice of Lindler, we used a particle hit threshold of 100σ, and a noisy diode threshold of 4σ for all the data analysed. A series of test datasets were analysed and run through both the STSDAS version of "`parthity`", and the prototype version of that task written in IDL by Lindler. The resulting dark count-rates were identical, and the "quantization" disappeared.

We then used the STSDAS task "`hstpos`" and the SHH files to find the geographic position of HST at the start of the integration for each frame (or more properly group) in the dataset. From there the output from this step was sent through the STSDAS task "`geo2mag`", where the geographic co-ordinates are converted to geo-magnetic co-ordinates. This latter step is a simple spherical rotation from the geocentric coordinate system where the north pole is located at 90° latitude, 0° longitude, to the geo-magnetic co-ordinate system where the geo-magnetic north pole is located at 78.6° latitude, 289.3° longitude. There is no physics involved in this co-ordinate transform.

The last step used a specially coded task from J. Eisenhamer and the SHH files that calculated the great-circle distance between the (α, δ) of the pointing of HST's V1 axis, and the (α, δ) of the Sun at the start of each frame in each dataset. We call this final quantity the solar angle.

All these data (count-rates, positions, times, solar angles) were collated, and various correlations between variables explored.

5 Results

It is immediately apparent that the count-rates found from all the datasets in proposal 2748 were anomalously high – one order of magnitude larger on the RED side and two orders of magnitude larger on the BLUE side. On investigation, it was found that proposal 2748 was used to map the outline of the South Atlantic Anomaly (SAA). These datasets were therefore omitted from the calculations for the overall dark count-rates, and any of the correlations found between the variables. We also found that there were 71 datasets from proposal 1316 which have a count-rate of zero. On closer inspection, it turned out that the high voltage was not turned on. Again, we have omitted these datasets for further analysis. The average dark count-rates for each cycle by detector are given in Table 2.

Table 2: Dark count-rates by Cycle and detector

Cycle Number (Proposal)	Detector	Dark Count-rate (cts/sec/diode)
1 (1316)	RED	0.00914 ± 0.0032
1 (1316)	BLUE	0.00615 ± 0.0027
1 (1533)	RED	0.0125 ± 0.0027
1 (1533)	BLUE	0.00676 ± 0.0009
2 (2748)	RED	0.188 ± 0.27 (in SAA)
2 (2748)	BLUE	0.113 ± 0.16 (in SAA)
3 (4698)	RED	0.00834 ± 0.0039
3 (4698)	BLUE	0.00546 ± 0.0023
SMOV (4773)	RED	0.0134 ± 0.0054
4 (5532)	RED	0.0107 ± 0.0038
4 (5532)	BLUE	0.0074 ± 0.0028

The overall average dark count-rate is 0.0109 ± 0.0022 cts s^{-1} diode^{-1} for the FOS/RED, and 0.0064 ± 0.00083 cts s^{-1} diode^{-1} for the FOS/BLUE.

In Figure 1 we plot in $5^\circ \times 5^\circ$ bins the dark count-rate for the FOS/RED (top) and the FOS/BLUE (bottom). These plots are superimposed upon an equal-area projection of the Earth. The roughly $\pm 40^\circ$ band centered on the equator is the orbit of HST. It is apparent on both plots that the area over South America and the south Atlantic are regions of elevated counts (the SAA). We also note that the SAA for the FOS/RED is about half again as large as the SAA measured with the FOS/BLUE. The results for the FOS are very close to those found by the GHRS team for their Digicons (see Lindler 1995).

We explored any possible correlations in the various quantities we had compiled (*i.e.* position, solar angle, and time). We found the following relationships to be true:

1. Using singular value decomposition (SVD), there is **no** time dependence for the dark count-rates. To within 1σ, for both the FOS/RED and FOS/BLUE, the count-rates are flat. We show this in Figure 2, where we have plotted all the non-SAA impacted dark count-rates versus the time since launch of HST. We see no evidence for a trend in the data. There may be a hint of an increase in the dark count-rates in the post-COSTAR compared to the pre-COSTAR data, but it is not compelling. We do note the consistent, and expected finding that the RED dark count-rate is systematically larger than the BLUE dark count-rate. This latter result is expected as the FOS/RED detector is not as well shielded against external magnetic fields as is the FOS/BLUE.

2. Using SVD, there is **no** correlation between the solar angle and the dark count-rate, for either detector. In Figure 3 we have plotted the solar angle at roughly the middle of a given dataset's exposure time against its mean count-rate. This leads to rather misleading hard edges in the data plotted. What is of more interest is the spead in values of dark count-rate at a given solar angle. As we do not distinguish at what epoch the darks were taken, nor geo-magnetic position, this spead it not unexpected. We did look for any correlations between the solar angle and the geo-magnetic position and found no trends in the data. We do note that the BLUE count-rate is systematically lower than the RED detector, as expected.

3. Using SVD, there is **no** correlation between geo-magnetic longitude and dark count-rate, for either detector. In Figure 4 we have plotted the data for all the darks, and aside from the characteristic systematic differences between the BLUE and RED sides, we find that both sides have no correlation with the geo-magnetic longitude. We note that the scatter for the RED side is substantially larger for that of the BLUE. This is explained partly by the fact that there are only 84% as many BLUE darks as RED ones, and partly from the known problem that the RED detector is not as well magnetically shielded as the BLUE. We submit that some of the scatter is due to poor RED side shielding. When the data are analysed using SVD, we found that there is no simple closed-form relationship (*i.e.* polynomial form) between the dark count-rate and geo-magnetic longitude – the data are essentially flat even when using REAL*8 arithmetic. We also found that smoothing the data had had no effect, other than to reduce the scatter.

4. Again, using SVD, we confirm the finding of Rosenblatt *et al.* of the relation between geo-magnetic latitude and dark count-rate. We have chosen a parabolic (*i.e.* second order) relationship for the geo-magnetic latitude *vs* dark count-rate, for both detectors. The relationship for the FOS/RED is (in cts s^{-1} diode^{-1})

$$\mathrm{Rate}_{\mathrm{Red}} = 8.8 \times 10^{-3} - 8.0 \times 10^{-6}\lambda_{gm} + 5.2 \times 10^{-6}\lambda_{gm}^{2},$$

   and for the FOS/BLUE (in cts s^{-1} diode^{-1}) is

$$\mathrm{Rate}_{\mathrm{Blue}} = 4.3 \times 10^{-3} + 3.0 \times 10^{-5} \lambda_{gm} + 3.0 \times 10^{-6} \lambda_{gm}^2.$$

The data are plotted in Figure 5. We note that there is a good deal of scatter in the plot – leading to a fair amount of overlap between the FOS/RED and FOS/BLUE datasets. As we have not differentiated the programmes in any way in this plot, the scatter should not be too surprizing. What we have is an integration of the darks over the last 1800 days, taken at various points in the Solar cycle. Indeed 1990/91 was the peak of the current Solar cycle, while 1995 (the last data in this study) is trailing off to the Solar minimum.

6 Discussion

Having found overall relationships between the FOS dark count-rate and primary observables (*i.e.* simple measured quantities in the data), we now look to see if there are any second order effects. In the class of second order effects, we include any possible relation between the dark count-rates of the FOS/BLUE and the FOS/RED, where there exist observations on both detectors within 1° boxes. Somewhat surprisingly, for the number of datasets, there are less than 50 simultaneous FOS/BLUE and FOS/RED matchings. It turns out that under Bayesian statistics we should expect to see only 31 matches. These matches are plotted in Figure 6, and shows no discernible correlation. This is as expected (and hoped) as this tells us there is no electronic cross-talk between the two detectors. We note that there exists a linear relation between the two detectors on the GHRS (Lindler 1995), and knowing this to be true for GHRS, decided to see if such a relation exists for the two FOS detectors.

As we mentioned in the Results section above, we have not taken into account any information concerning the Solar cycle. Referring back Figure 2, we find that the current Solar maximum was between 1989 and 1992, with all the observations from proposals 1316 and 1533 occuring during 1990 and 1991. (On Figure 2, these occur below Day 550). By inspection there is no apparent correlation between the Solar activity – it is comparable in level and scatter to the data from proposal 5532 (Cycle 4), which data were obtained in 1995 at the minimum of the current Solar cycle. The upshot is that we see no evidence of a connection between the dark count-rate and the Solar activity.

7 Models

Currently the FOS dark count-rate is modeled in the OPUS pipeline using a lookup table generated from the SV/OV analysis based on proposals 1316 and 1533. This table has entries for both the FOS/RED and FOS/BLUE detectors in $5^\circ \times 5^\circ$ bins of geo-magnetic position, and uses a simple interpolation technique estimate a value, and subtracts this value from count-rate spectra being processed in the pipeline using the STSDAS task "`calfos`".

The starting point for the interpolation is based on the geo-magnetic longitude and latitude of the dataset, found in the science data header line. However, the data upon which the lookup table is based is from the SV/OV epoch only. We anticipate that a longer baseline in time may give an improvement to the model.

In Figure 7, we plot the averaged FOS/RED dark count-rate in $5^\circ \times 5^\circ$ bins of geomagnetic position. All the data from the SAA are ignored. The top part of the figure shows the raw bins while the bottom part shows 2 smoothed 1-dimentional cubic spline fits to the binned data. The first spline fits the dark count-rate *vs* the binned geo-magnetic latitude and the second spline fits the residual dark count-rate (*i.e.* the binned data with the first spline fit subtracted away) *vs* geo-magnetic longitude. The two fits were then combined to form the model. Figure 8 shows the same pair of plots for the FOS/BLUE. In both of the figures, the most significant deviation is found in the geo-magnetic latitude, with roughly double the counts at high geo-magnetic latitudes than at the geo-magnetic equator.

In the top panels of Figures 9 and 10, we plot the average dark count-rate (the triangles) *vs* the geo-magnetic latitude with a 2σ error bar (*i.e.* twice the standard deviation about the averages). Over these, we plot a model of the dark count-rate defined by a least-squares cubic spline fit with 9 nodes.

The variations in the binned data as modeled by the cubic spline *vs* geo-magnetic latitude are subtracted from each $5^\circ \times 5^\circ$ average dark. The lower panels in Figures 9 and 10 show the residual average dark count-rate *vs* geo-magnetic longitude. Another least-squares cubic spline was fit to these points, and used as a model (the solid line). To avoid discontinuities in the models between 0° and 360° the data were fit 3 times: one with the actual geo-magnetic longitude; one with the geo-magnetic longitude - 360°; and one with the geo-magnetic longitude + 360°. The cubic spline used had 24 nodes.

An important comparison to make is how does the FOS dark count-rate compare with that measured by the GHRS. This is a reasonable comparison to make as both instruments use Digicons as the photo-electron detectors. We have plotted the FOS and GHRS dark count-rate models to the same scales in Figures 11 and 12, and find that both instruments exhibit to a remarkable degree, very similar characteristics for both the RED and BLUE detectors, and in the way these detectors respond to the particle background at various geo-magnetic positions. Figure 11 shows the comparison between the FOS/RED and the GHRS RED, while Figure 12 shows the same data for the FOS/BLUE and GHRS BLUE. We note especially that for the residual models of the geo-magnetic longitude, both the FOS and the GHRS have the shapes, even down to the wiggles at geo-magnetic longitude 60°. The amount of scatter, and the magnitude of the variation are the same in both sets of plots. The differences in the spline fits are most likely due to the slight response differences of the individual tubes, and shielding in the instruments. The conclusion for both the GHRS and the FOS is that the dominant affect on the dark count-rate is changing geo-magnetic latitude, and there is a very weak (2% effect) due to geo-magnetic longitude. It is on the basis of this analysis that the lookup table used by the current FOS pipeline was generated.

Comparing the least-square fits we made in this study with the current pipeline models.

The curves are plotted in Figure 13; with the top pair being the FOS/RED, and the bottom pair for the FOS/BLUE.

For the FOS/RED, the pipeline model (dot-dash line) is quite asymmetric, having a very steep rise for geo-magnetic latitude < $-15°$. Compared with the parabolic model (dashed line), the pipeline model is $\sim$ 20% higher at geo-magnetic latitude = $-40°$, and $\sim$ 26% lower than the parabolic model at geo-magnetic latitude = 40°. In the region $\pm 20°$, the two models are well matched.

The models for the FOS/BLUE are more problematic. The pipeline model (dot-dot-dot-dash line) is flat, while the parbolic fit (solid line) is also flat, but skewed to the pipeline model. The parbolic fit is 7% lower than the pipeline for all geo-magnetic latitude < 10°, crosses over at geo-magnetic latitude = 18°, and is higher for geo-magnetic latitude > 20°.

An interesting execise to carry-out is to use the extreme deviations between the new models and the current OPUS pipeline models to see how these differences translate into FOS detector count-rates. The motivation being to see if one can really make significant changes to the calibrated photometry of the FOS by refining the dark count-rate models used in the HST pipeline calibrations. We anticipate that the differences in the models will lead to rather signifiant differences to the photometry of very faint (V $\sim$ 21) sources, in either detector. To this end, we have simulated as series of "standard" targets at various magnitudes through 2 different gratings on both detectors. We note immediately that for targets at V = 15, the changes in the net count-rate are very small – indeed insignificant, but for objects between V = 17 and V = 19, the changes start to become important – on the order of a few tenths of a percent. At V = 21, the variations in dark count-rate become very large and very significant – in some cases the photometry can vary by up to 10%! As these "standard" objects are all high (*i.e.* > 30) S/N data, one can also see that for more moderate S/N data, the photometric effects will be even more serious. In fact, because fainter objects usually have lower S/N, this effect may dominate the data in those cases.

8 References

Rosenblatt, E.I, Baity, R.W., Beaver, E.A., Cohen, R.D., Junkkarinen, V.T., Linsky, J.B., and Lyons R.; 1992 CAL/FOS 071 "*An analysis of FOS background dark noise*" (Baltimore:STScI)

Beaver, E.A., and Lyons, R.W.; 1992 CAL/FOS 076 "*Analysis of FOS On-orbit detector background with burst noise rejection*" (Baltimore:STScI)

Lindler, D.J.; 1995 in **Calibrating HST: Post Servicing Mission** eds A. Koratkar and C. Leitherer, p 216 (Baltimore:STScI)

Table 3: Change in FOS count-rates as a function of "standard" template objectand magnitude. All entries are in percentage change in simulated FOS counts between the extreme differences between the current FOS dark count-rate models and the new models presented in this study.

Object	Detector			
	FOS/RD		FOS/BL	
	G190H	G400H	G130H	G400H
O7V				
V=15	0.01%	0.01%	0.008%	0.001%
V=19	0.4%	0.3%	0.3%	0.01%
V=21	2.0%	2.0%	1.0%	0.3%
A1V				
V=15	0.3%	0.02%	0.05%	0.005%
V=19	5.0%	0.8%	1.0%	0.2%
V=21	9.0%	4.0%	1.5%	0.7%
M2I				
V=15	–	0.2%	–	0.06%
V=19	–	0.9%	–	0.9%
V=21	–	1.3%	–	8.0%
QSO ($\alpha = 1$)				
V=17	0.1%	0.02%	0.1%	0.05%
V=19	0.4%	0.8%	0.6%	0.1%
V=21	4.0%	7.0%	1.0%	1.0%
Flat ($\alpha = 2$)				
V=15	0.2%	0.03%	0.3%	0.01%
V=21	9.0%	5.0%	2.0%	1.0%
T=50000K				
V=15	0.01%	0.01%	0.005%	0.002%
V=21	2.0%	2.0%	0.7%	0.4%
PN				
V=17	–	0.03%	–	0.02%

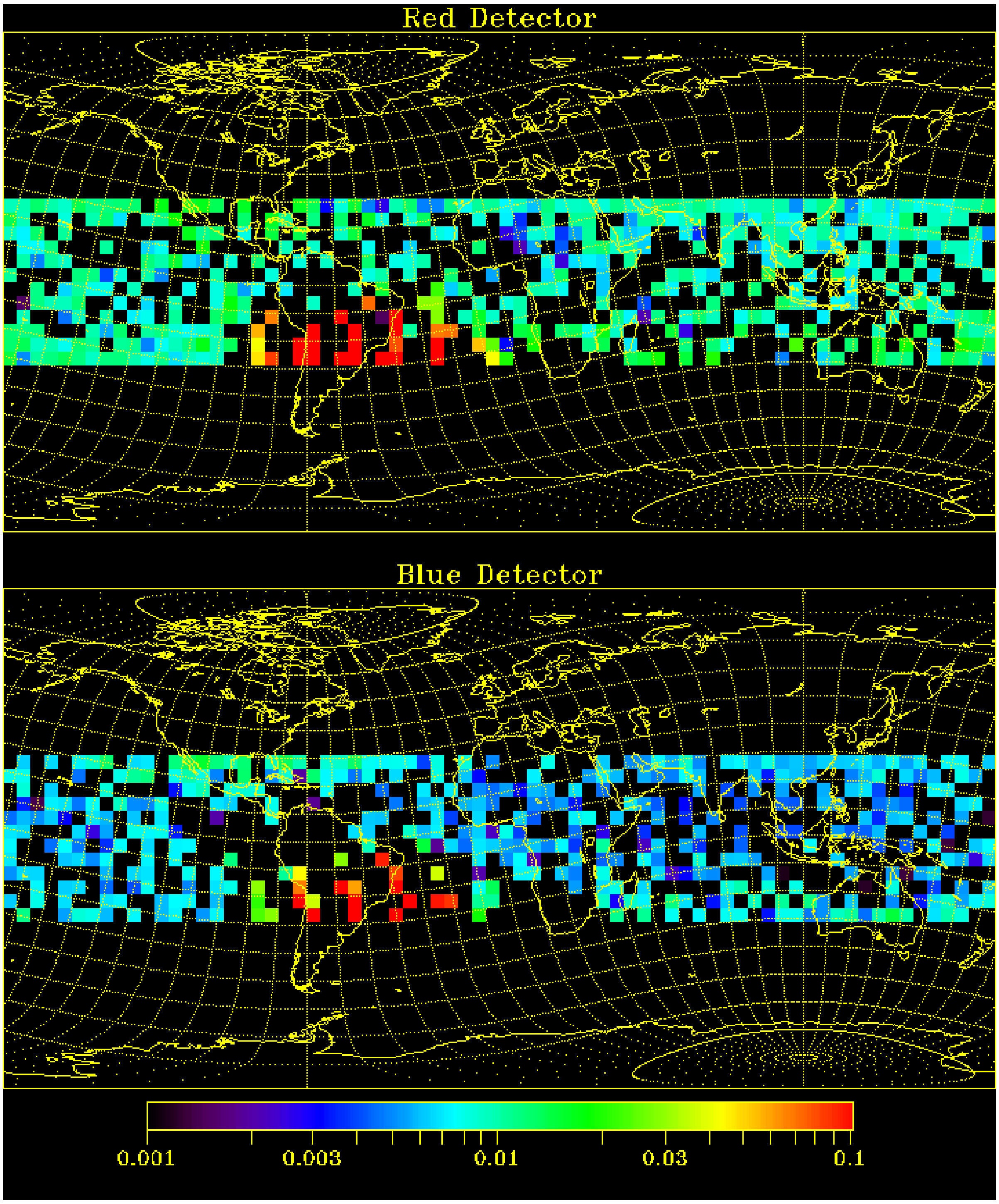

Figure 1: Plot of dark count-rate in $5^{\circ} \times 5^{\circ}$ bins superimpos ed on the Earth. The top plot is for the FOS/RED, while the bottom plot is for the FOS/BLUE. Over South America and the south Atlantic is the SAA; the SAA measured by the FOS/RED is substanitially larger than that measured by the FOS/BLUE.

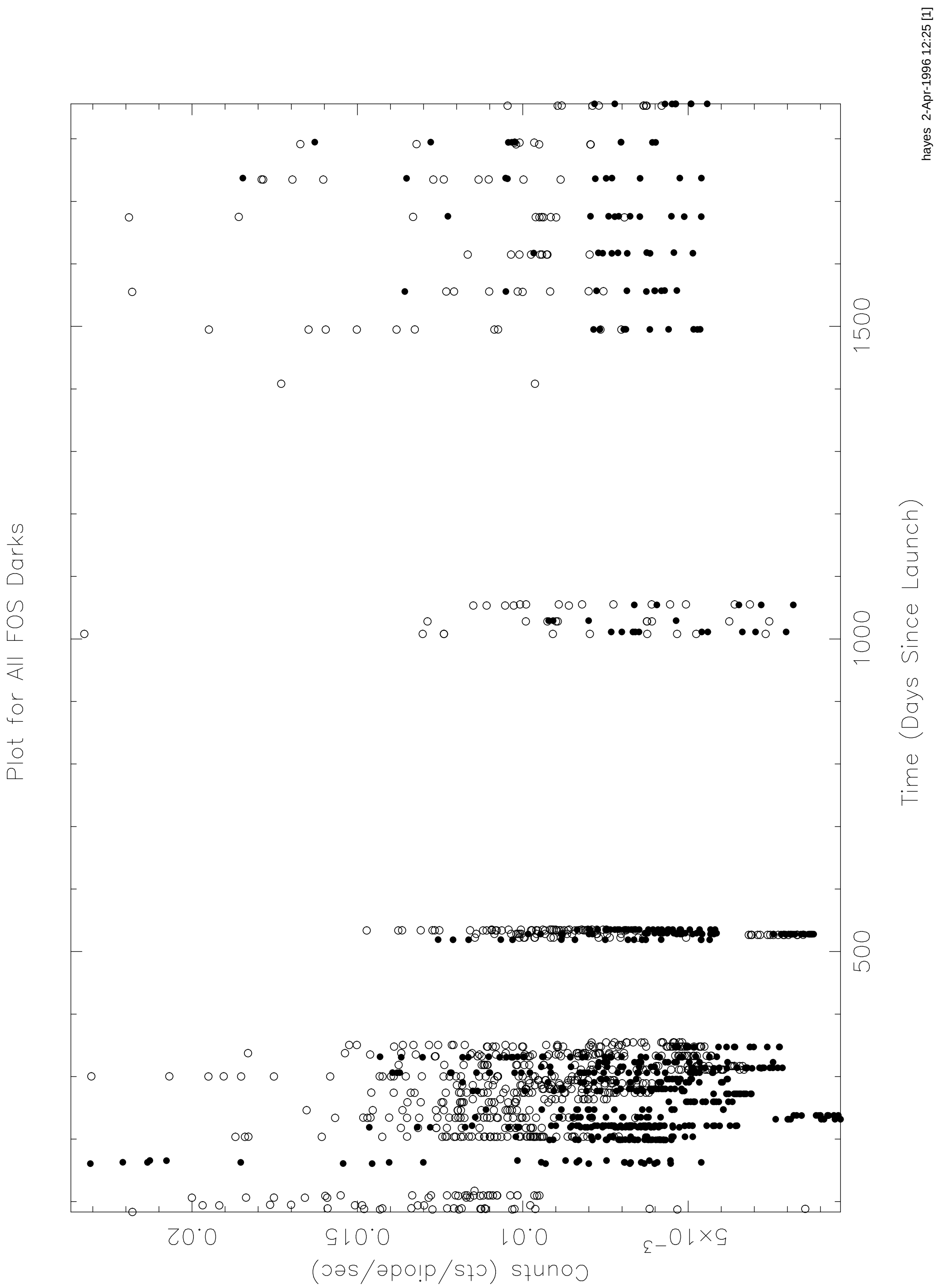

Figure 2: Plot of dark count-rate *vs* Days since launch. Open symbols are FOS/RED datasets and filled symbols are FOS/BLUE datasets.

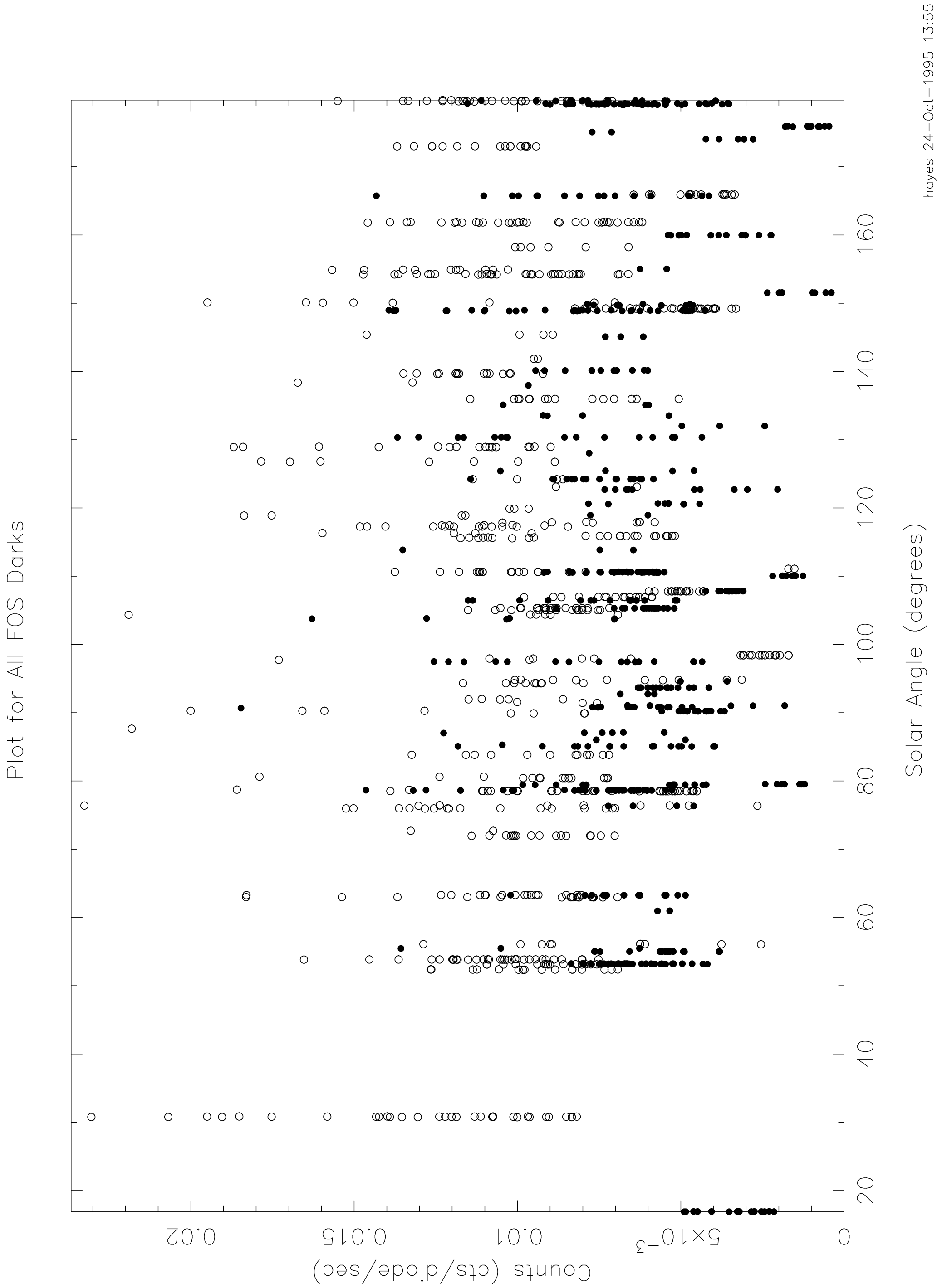

Figure 3: Plot of dark count-rate *vs* Solar angle of HST. Symbols have the same meaning as in the previous figure.

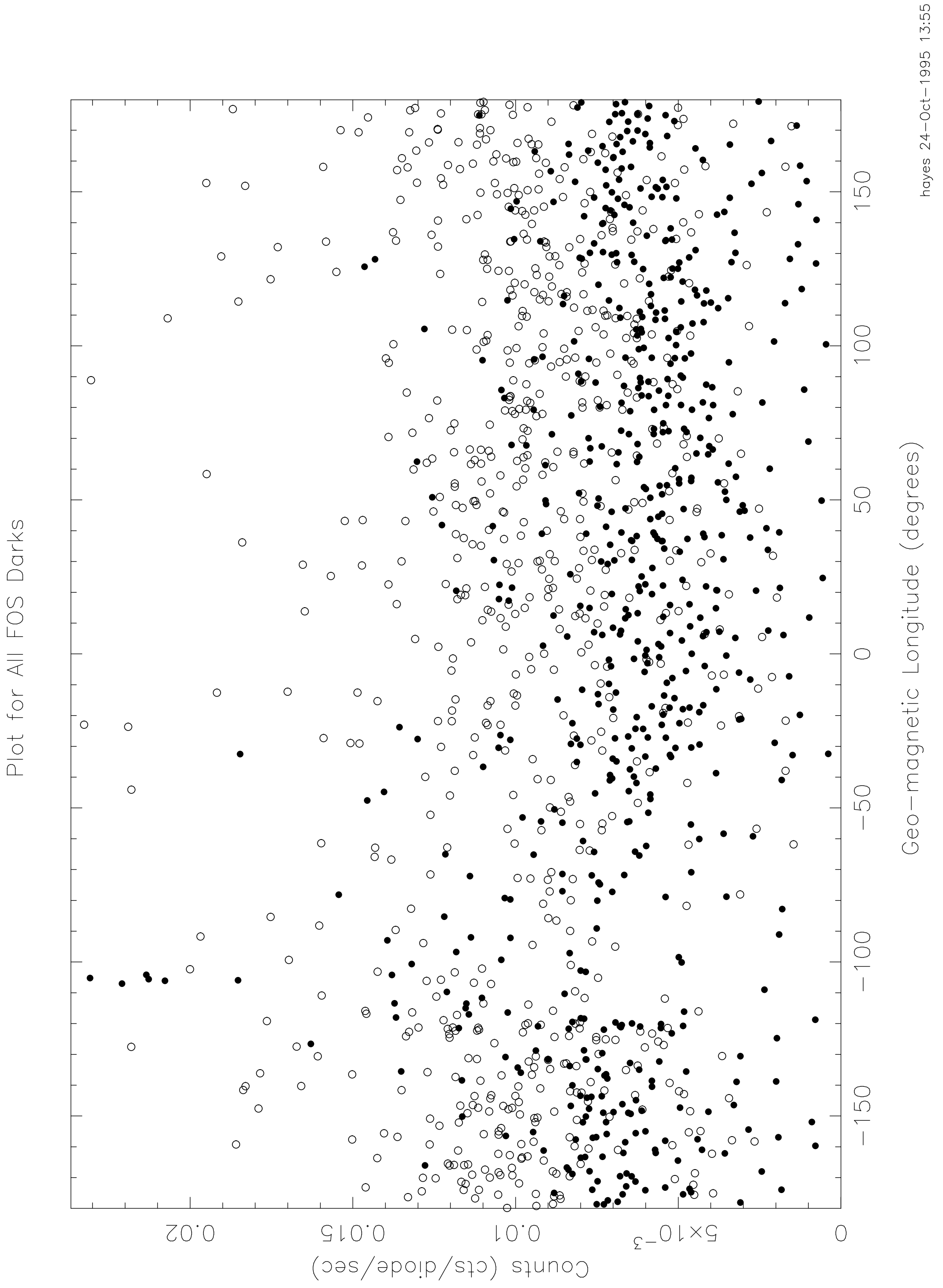

Figure 4: Plot of dark count-rate *vs* geo-magnetic longitude. Symbols as in the previous figures.

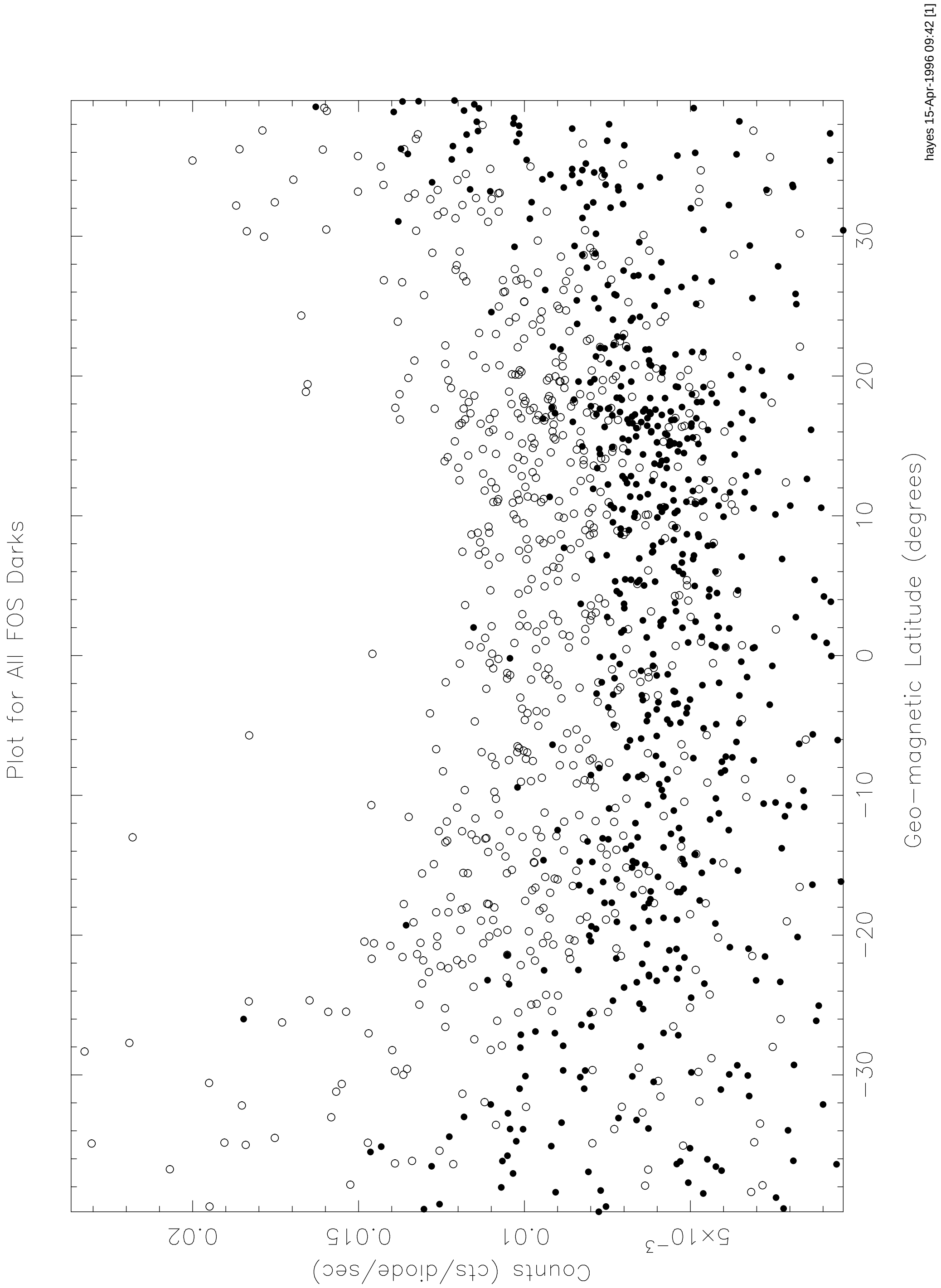

Figure 5: Plot of dark count-rate *vs* geo-magnetic latitude. The symbols have the same meaning as in the previous figures.

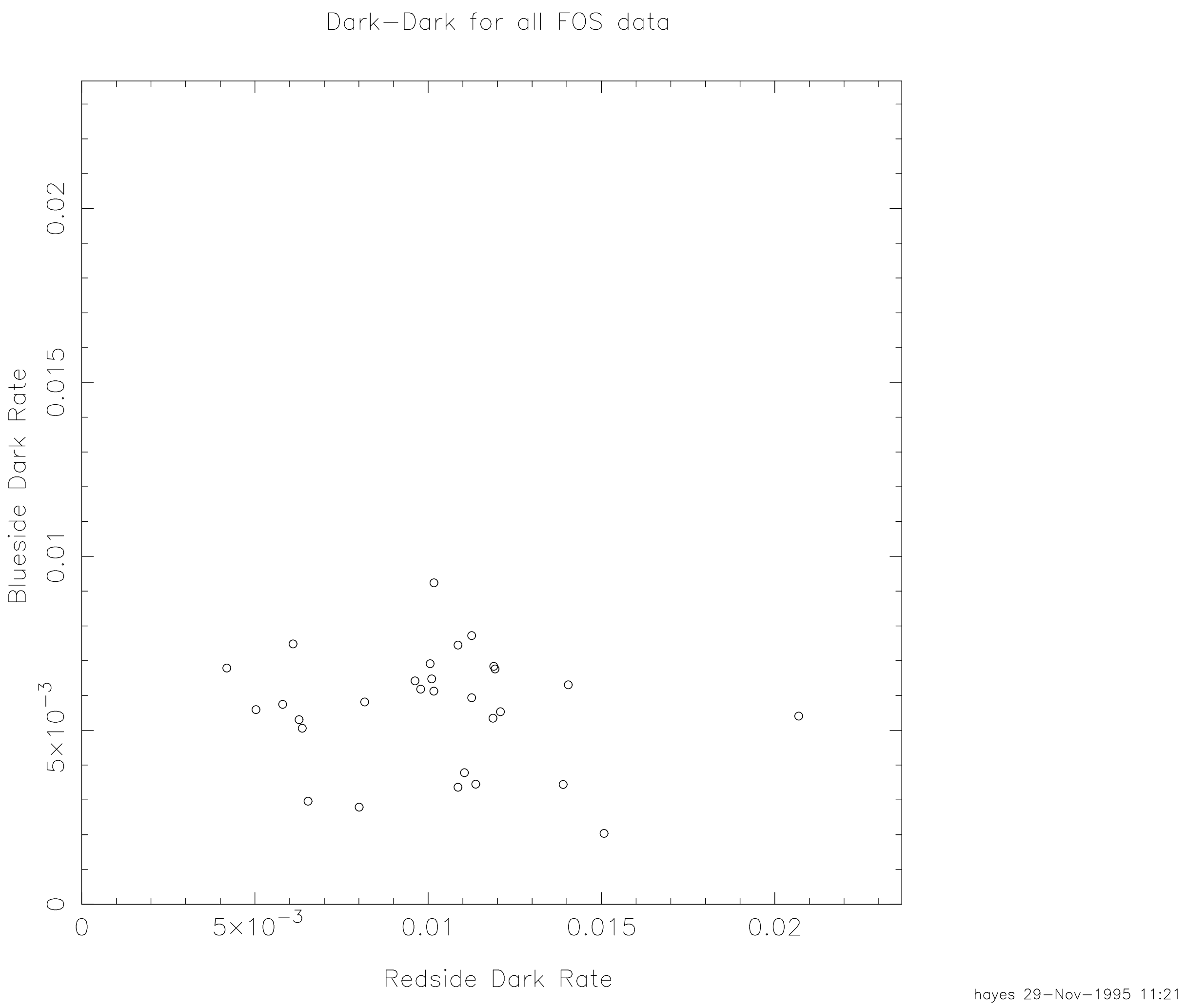

Figure 6: Plot of the BLUE *vs* RED dark count-rates.

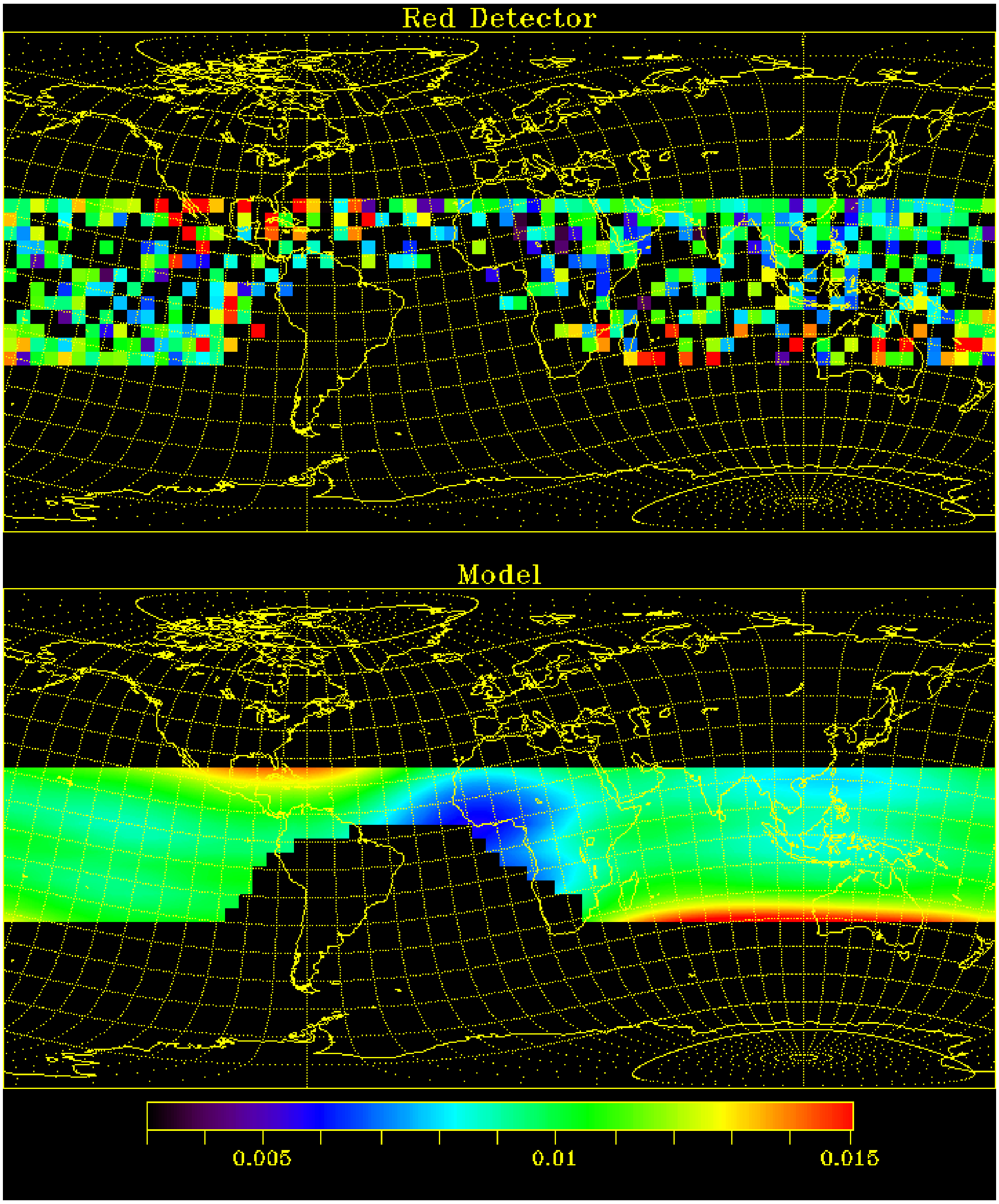

Figure 7: Averaged FOS/RED dark count-rate in $5^\circ \times 5^\circ$ bins s uperimposed on the Earth. The top plot is the 'raw' data, while the bottom is a smoothed 2-dimentional spline fit to the binned data.

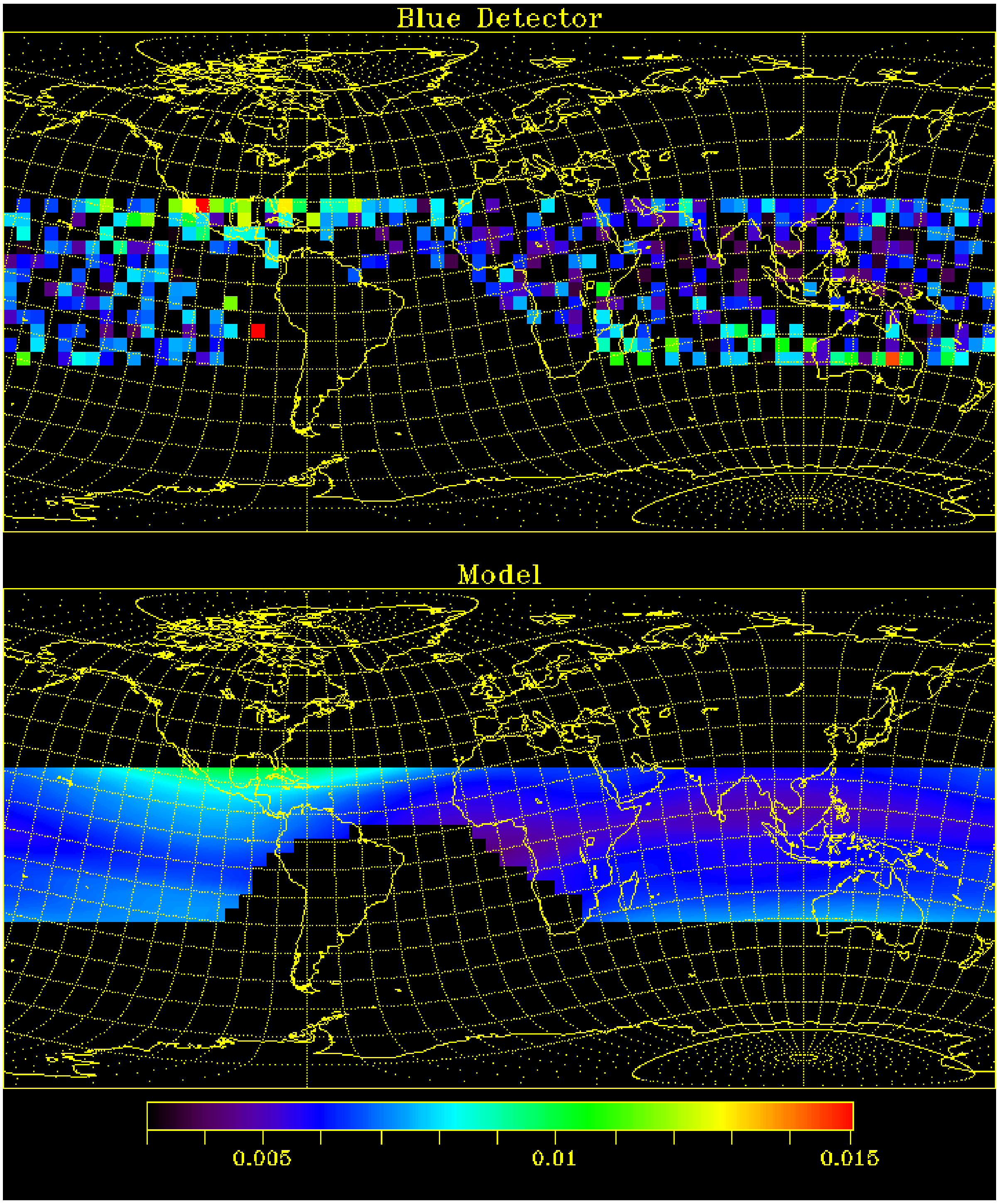

Figure 8: Averaged FOS/BLUE dark count-rate in $5^\circ \times 5^\circ$ bins superimposed on the Earth. The top plot is the ‘raw’ data, while the bottom is a smoothed 2-dimentional spline fit to the binned data.

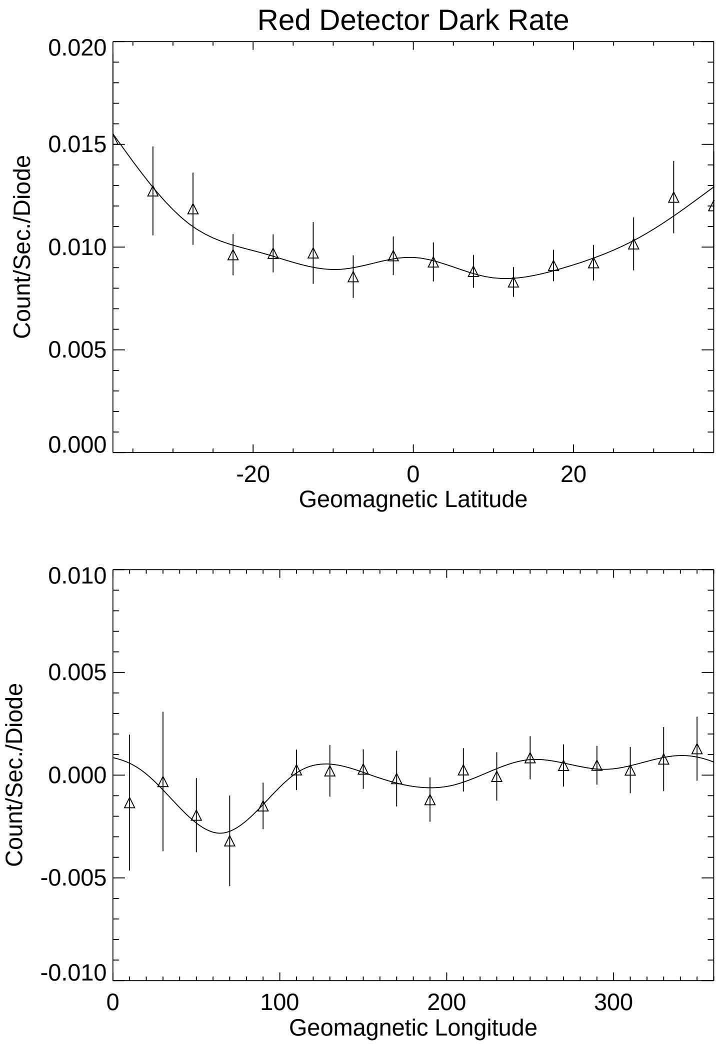

Figure 9: Least-squares cubic spline fits to averaged FOS/RED geo-magnetic positions. The top panel is the fit for geo-magnetic latitude, while the bottom panel is of geo-magnetic longitude. The error bars are 2σ in size.

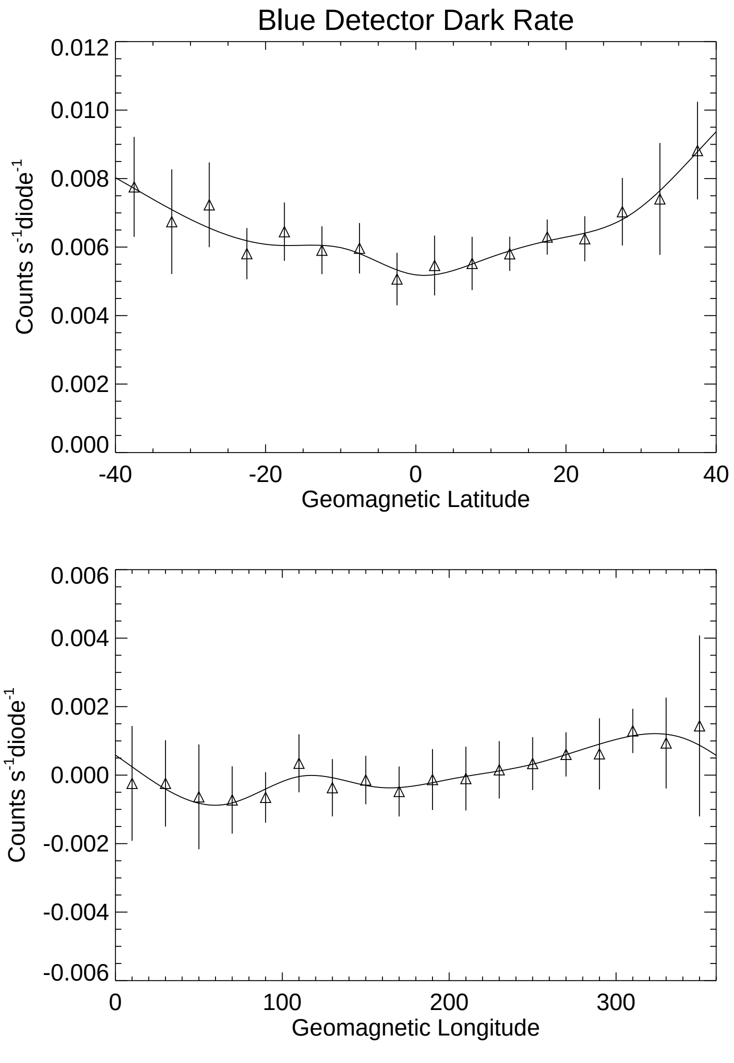

Figure 10: Least-squares cubic spline fits to averaged FOS/BLUE geo-magnetic positions. As in the previous figure, the top panel is the fit with geo-magnetic latitude, while the bottom panel is of geo-magnetic longitude. The error bars are 2σ in size.

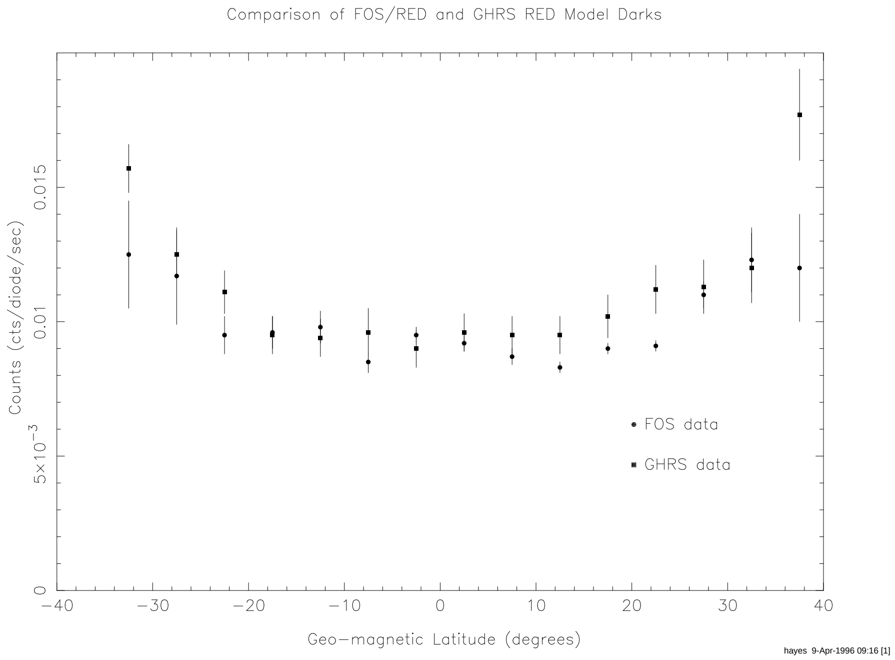

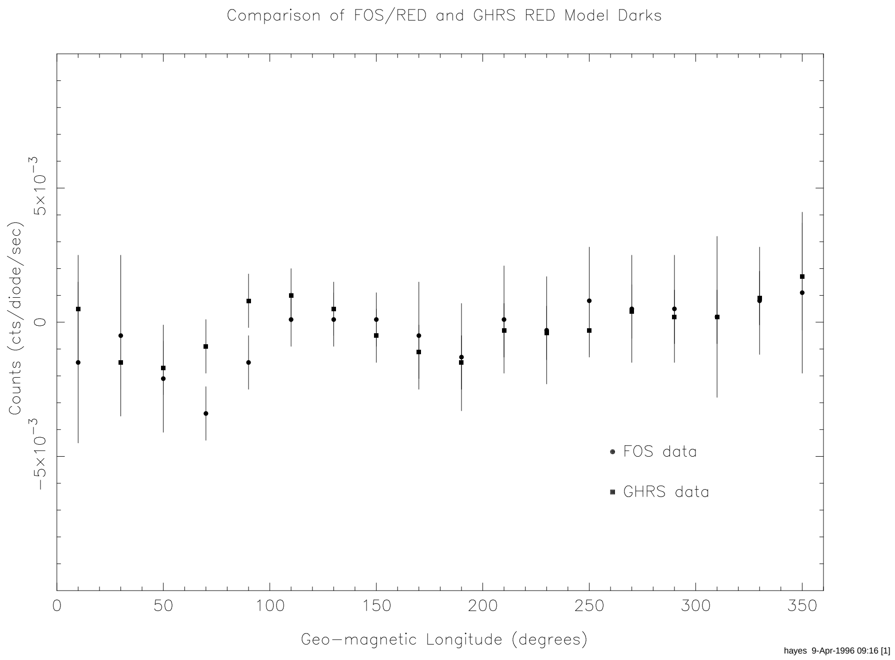

Figure 11: Comparison of the FOS/RED and GHRS RED dark count-rate models. The top panel shows the count-rate *vs* geo-magnetic latitude, and the bottom panel shows the count-rate *vs* geo-magnetic longitude. We note the very similar shapes and scatter in both science instruments.

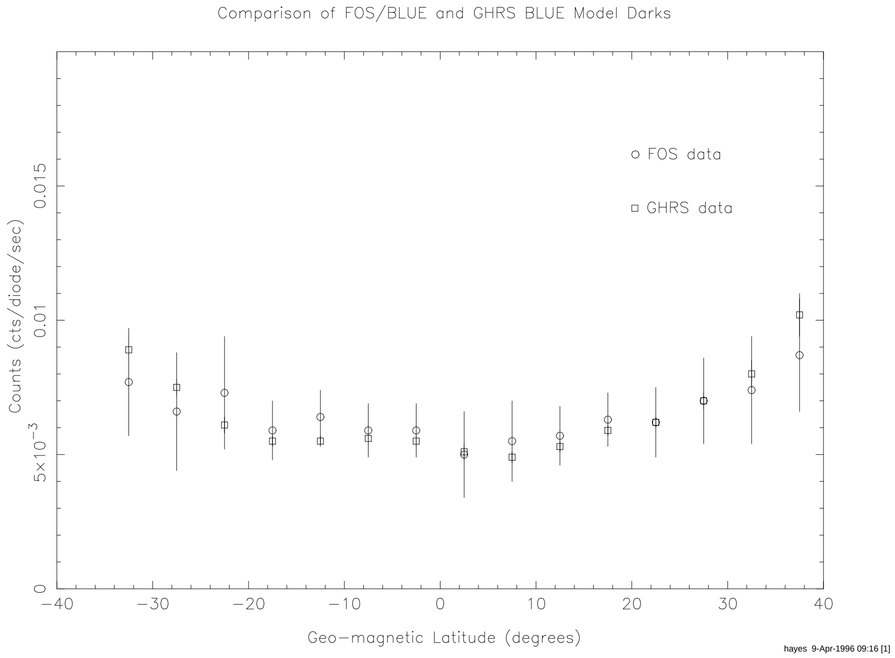

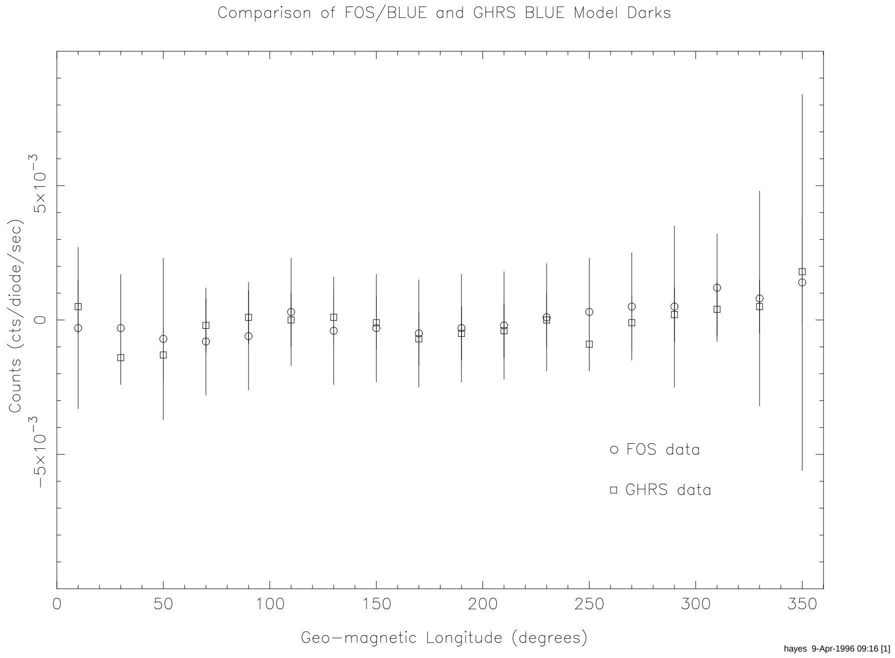

Figure 12: Comparison of the FOS/BLUE and GHRS BLUE dark count-rate models. The top panel shows the count-rate *vs* geo-magnetic latitude, and the the bottom panel shows the count-rate *vs* geo-magnetic longitude. As in the previous figure we note the very similar shapes and scatter in both science instruments.

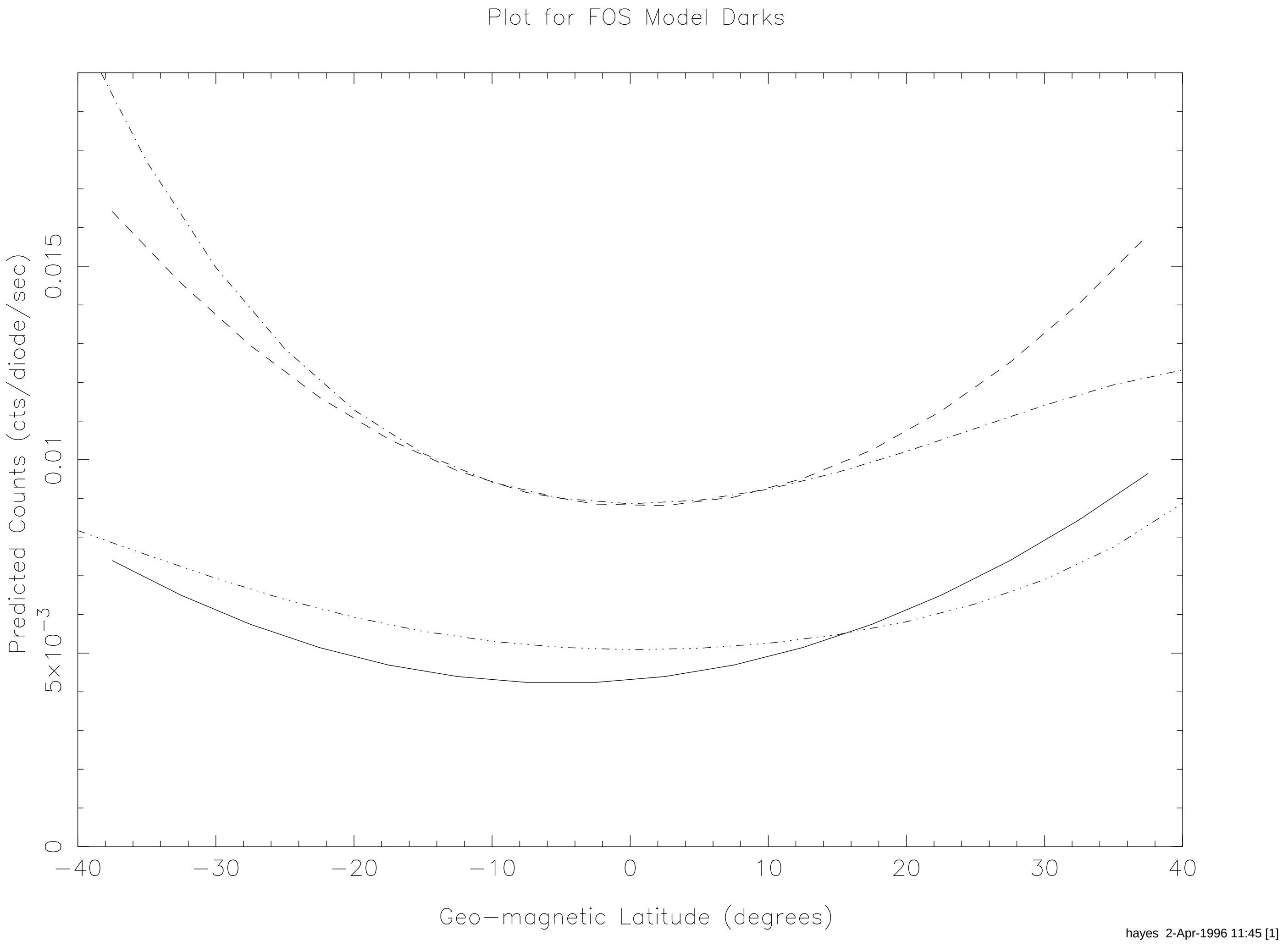

Figure 13: Comparison of OPUS pipeline models (cubic splines) with parabolic fits from this study. The top pair of curves are for FOS/RED: dot-dashed line is pipeline model; dahed curve is parabolic fit. The bottom pair of curves are for the FOS/BLUE: dot-dot-dot-dashed curve is the pipeline model; solid curve is the parabolic fit.